2014 Canada-China Conference on Advanced Reactor Development (CCCARD-2014)
Niagara Falls Marriott Fallsview Hotel & Spa, Niagara Falls, Ontario Canada, April 27-30, 2014.

CCCARD2014-009

PHENOMENOLOGICAL INVETIGATION AND NUMERICAL SIMULATION OF GAS BUBBLE BEHAVIORS IN THE VICINITY OF MIXING VANE OF SPACER GRID

J.Y. Zhang [1], X. Yan [1] and J.J. Xu [1]
[1] CNNC key laboratory on reactor thermal hydraulics technology, NPIC, Chengdu, China

Abstract

Visualization technique was adopted to study gas bubble behaviors in the vicinity of mixing vane of spacer grid in a 3×3 rod bundle under ambient temperature and atmospheric pressure. It was found that bubble stagnation, which was dependent on liquid flow rate or volume fraction, occurred at the leeward of mixing vane, influencing the bubble size and phase distribution in the bundle. In the numerical simulation, VOF method was implemented to tracking bubble interface in a typical subchannel. Good agreement was found between experiment and numerical simulation. The influence of bubble behaviors on pressure drop was also investigated.

1. Introduction

The spacer grid with mixing vanes of PWR fuel assembly is designed to enhance heat transfer and CHF by introducing strong turbulence into the coolant. The thermal-hydraulic performance of spacer grid is of great significance to the economics and safety of the reactor core. Much attention have been paid on the studies of the flow process in the rod bundles with spacer grid to improve the understanding of the physical mechanism, in which the two phase flow has been more concerned to obtain beneficial experiment data and to develop reasonable model despite the complexity of the two phase flow. However, little attention was paid on the local phenomena around the spacer grid, especially in the vicinity of mixing vane, which has specific influences on the phase distribution at the downstream of the spacer grid and the flow pressure drop of the bundle. Hence, it is necessary to consider the bubble behaviors in the vicinity of mixing vane by conducting visualization experiment to achieve useful information of the local phenomena.

Volume of Fraction model(VOF) proposed by Hirt and Nichols [1] is a kind of interface tracking technique and has been implemented in the simulation of bubble dynamics [2], break-up [3], coalescence [4], evaporation [5], condensation [6] and sliding [7] owing to its easiness to operate and good conservativeness. With the help of VOF method, it is possible to achieve detailed information of phase interface and local phenomena by simulating the behaviors of bubbles passing the spacer grid.

In this study, visualization experiment and numerical simulation with VOF method were carried out to examine the gas bubble behaviors in the vicinity of mixing vane of spacer grid. The influence of bubble behaviors on pressure drop of the subchannel was also investigated.

2. Experimental method

2.1 Experimental facility

The visualization experiment was carried out in the open loop with ambient temperature and pressure at Nuclear Power Institute of China (NPIC). As shown in Figure 1, the experimental facility consisted of a circulation pump, two venturi flowmeters, a test section, a water tank, a compressor and two aerometers. The liquid flow rate of test section was controlled by a bypass valve and regulator valves. The gas to generate bubbles was provided by a compressor and governed by micro-metering valves. The visualization system was composed of a Phantom V9.0 digital high speed camera of US York, data processing system and main and auxiliary illumination systems which were employed to enhance the lightness around mixing vanes of spacer grid.

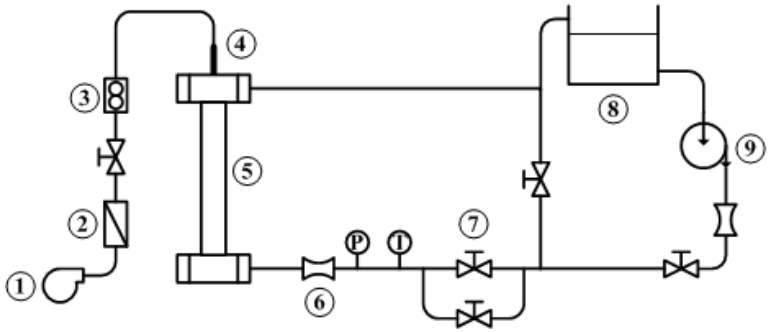

(1) Compressor, (2) air filter, (3) aerometers, (4) injecting rod, (5) test section, (6) venturi, (7) regulator valves, (8) water tank, (9) circulation pump.

Figure 1 Schematic of the experimental facility.

2.2 Test section

The test section included the inlet and outlet headers, the flow housing and the rod bundle. A vertical 41×41mm^2 square channel was formed by four pieces of plexiglass which were also used as the visualization windows. A 3×3 rod bundle with 9.5mm rod diameter and 3.1 rod-to-rod gap was installed in the flow housing. The cross-section of test section is shown in Figure 2.

The Fluorinated Ethylene Propylene(FEP) rod was applied to keep the consistence of refractive index between water and transparent rods, minimizing the phase interface distortion through the bundle. The bundle with two spacer grids in the flow housing was 1300mm long, and the upstream grid was conditioner grid. A FEP tube with a 0.6mm hole was used as the gas injector to generate bubbles before spacer grid in the certain subchannel of the bundle. With the application of this gas injecting rod, which is shown in Figure 2, it was able to generate bubbles in specific subchannel such that it was possible to obtain available images of bubble behavior in the vicinity of mixing vane without the disturbance of interface

overlapping. The bundle was fixed and sealed up at the top of the outlet header of the test section.

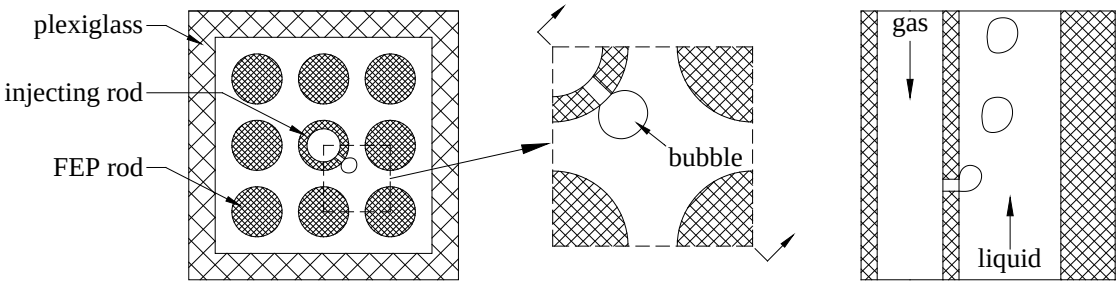

Figure 2 Cross-section of the test section and the injecting rod.

3. Numerical method

3.1 Computational geometry

The simulations of bubble behaviors were carried out in a typical subchannel with 9.5mm rod diameter and 3.1 rod-to-rod gap to limit the requirement of calculation resources and time. The subchannel with 180mm in length was derived from one of the subchannels of the bundle which was used in the visualization experiment as shown in Figure 3. Two mixing vanes were set reversely at the top of the strip. The gaps betweens the rods were treated as solid wall in the simulation. Simulations of bubbles moving at the windward and leeward of the mixing vane were performed with different initial conditions, which are shown in Figure 3.

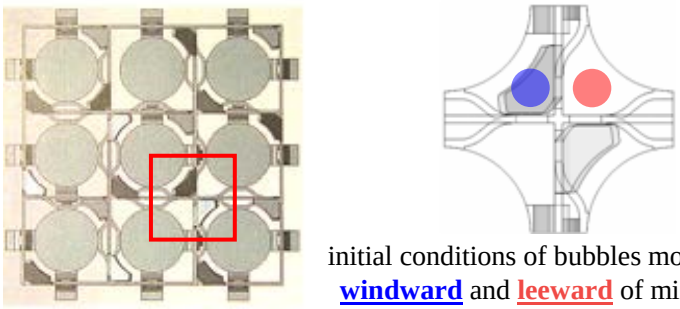

Figure 3 Diagram of the subchannel and bubble initial conditions.

3.2 Physical model

In the numerical simulation, VOF model was adopted to tracking phase interface with PLIC model [8] to reconstruct the phase interface. CSF model [9] was used to model the surface tension force of the interface.

3.2.1 VOF model

VOF model is based on that the two phases are not interpenetrating and can model different immiscible fluids by solving a single set momentum equations and tracking the volume fraction of each phase throughout the domain. In this model, an additional parameter, which is volume fraction of each phase, is introduced, and the variables and properties are volume averaged and are shared by each phase as the volume fraction in a cell is known.

VOF model solves the volume fraction continuity equation of one or multiple phases to capture the phase interface with the help of interface reconstruction model. For the gas phase in the two phase flow:

$$\frac{\partial \alpha_g}{\partial t} + \vec{u} \cdot \nabla \alpha_g = \frac{s_g}{\rho_g} \tag{1}$$

In the equation, s_g is the source term of gas phase, which is zero when phase change doesn't occur in the flow.

3.2.2 Surface tension model

With CSF model, the surface tension is calculated as a source term in the momentum equation. For the case that the surface tension is constant along the interface, it can be shown that the pressure drop across the surface depends on the surface tension coefficient σ, and the surface curvature measured by two radii in orthogonal directions, R_1 and R_2:

$$p_2 - p_1 = \sigma \left(\frac{1}{R_1} + \frac{1}{R_2} \right) \tag{2}$$

where p_i is the pressure of each side at the interface.

If n is the normal of the interface, α_q is the volume fraction of phase q:

$$n = \nabla \alpha_q \tag{3}$$

The curvature K is defined in terms of the divergence of the unit normal $\hat{n}$:

$$K = \nabla \bullet \hat{n} \tag{4-a}$$

$$\hat{n} = \frac{n}{|n|} \tag{4-b}$$

For the control volumes with two immiscible phases, the surface tension can be written as:

$$F_{vol} = \sigma_{ij} \frac{\rho K_i \nabla \alpha_i}{\frac{1}{2}\left(\rho_i + \rho_j\right)} \tag{5}$$

where ρ is the volume-averaged density of control volumes, which is defined in the VOF model.

3.3 Mesh scheme

In the simulation of hydraulic process in the rod bundle, hybrid mesh scheme was always employed to discrete the calculation domain due to the complexity of wall boundary. In the hybrid mesh scheme, unstructured and structural mesh were used in the region of spacer grid and rods, respectively. However, it was found that phase interface discontinuity occurred while the bubble was passing through the mesh interface between unstructured and structural mesh, as shown in Figure 4. Hence, polyhedral mesh scheme was adopted for the discretization to eliminate the discontinuity as well as to increase the solution efficiency by minimizing the total number of the mesh.

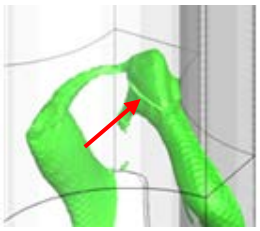

Figure 4 Phase interface discontinuity with hybrid mesh at the mesh interface.

The computational results are dependent on mesh density. The mesh should be fine enough to acquire the solution independent on the mesh number. In this study, mesh sensitivity analysis simulating single gas bubble rising in stagnated water was performed to determine the reasonable mesh size. By comparisons of phase interface and terminal rising velocity of rising bubbles among different mesh size, it was shown that the maximum mesh size of $0.1 \bullet D_b$ (bubble diameter) was acceptable in both calculation accuracies and mesh number. Different bubble diameters were observed in the visualization test including the diameter of 3mm, and the maximum mesh size in the simulation was set to 0.3mm, consequently.

4. Results and discussion

4.1 Experimental results and discussion

The spacer grid is designed to enhance heat transfer of fuel assemblies by introducing strong turbulence with mixing vanes. The bubble behaviors in the vicinity of mixing vanes, by which the phase distribution in rod bundle is influenced, are also characterized by the mixing vanes. In the visualization experiment, it was found that bubble stagnation, which was

dependent on the liquid flow rate and void fraction in the bundle, occurred at the leeward of the mixing vane. The behaviors of bubbles at the windward and leeward of mixing vanes had different influences on bubble size and bubble distribution at the downstream of the spacer grid.

Single bubble behavior was obtained to understand the basic characteristics of bubble movement. At the windward of mixing vane, the bubble rising up against the vane tended to sliding with expanding to both sides of mixing vane, and the ones close to the inner side of the vane tended to shift to the leeward of vane with bubble break-up, which is shown in Figure 5. At the leeward of mixing vane, the bubble came up into leeward of the vane and slided along the inclined vane with slowing its rising velocity.

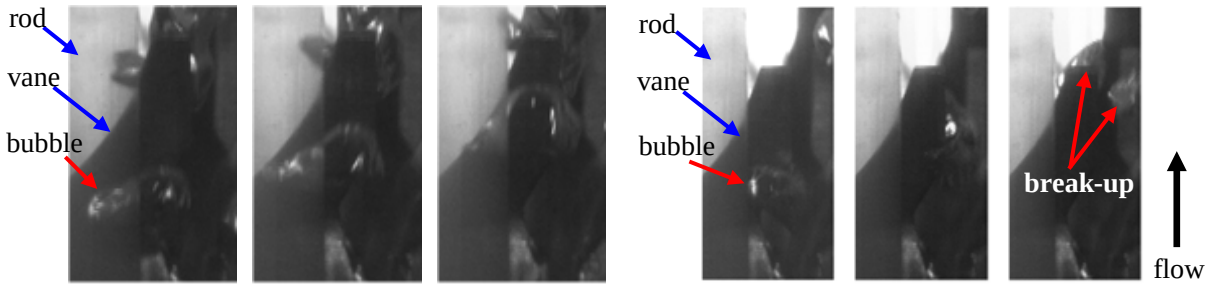

Figure 5 Photographs of single bubble behavior at the windward of mixing vane.

For multiple bubbles, it was difficult to control the location with continual gas injecting, which led to random bubble location to a certain extent. However, useful information was still achieved in the visualization experiment. At the leeward of mixing vane, bubbles stagnation occurred, forming a bubble with interface waving along flow direction, as Figure 6 shows. The inflow bubbles coalesced with stagnation bubble, which resulted in the instability of the stagnation bubble interface. The bubble break-up occurred as the interface instability transfer to the end of the stagnation bubble. Attributing to the instabilities induced by the bubble coalescence, the number of the break-up bubble at the downstream of the vane increased while the bubble size decreased comparing with the bubbles at the upstream of spacer grid, which indicated that bubble stagnation made a contribution to the bubble size varieties in the rod bundle. The configurations of inflow bubble and its post-break-up bubbles from the stagnation bubble are shown in Figure 7.

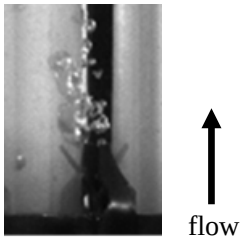

Figure 6 Photograph of bubble stagnation.

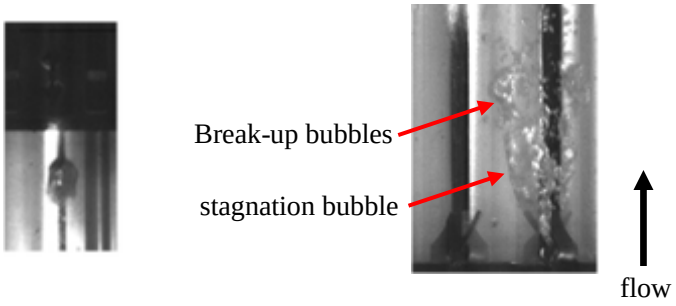

a. inflow bubble b. break-up bubbles

Figure 7 Varieties of bubble size in the rod bundle.

It was also observed that interface waving occurred due to the coalescence between the bubbles at the leeward of mixing vane and stagnation bubbles, which resulted in that the bubble breaking up from the stagnation bubble moved to the same direction as that the vane inclined to, which is shown in Figure 8. However, the interface waving caused by the coalescence between the bubbles at the windward of mixing vane and stagnation bubbles was against to the mixing vane. After the bubble broke up from the stagnation bubble, it moved to the other side of subchannel, which is shown in Figure 9. It indicated that the bubble behaviors at the windward and leeward of mixing vane yield to different bubble movement and phase distribution at the downstream of spacer grid.

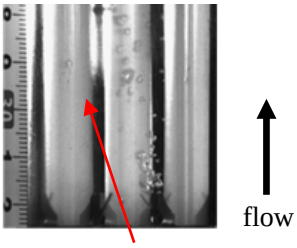

Figure 8 Photograph of the movement of bubbles from the leeward of mixing vane.

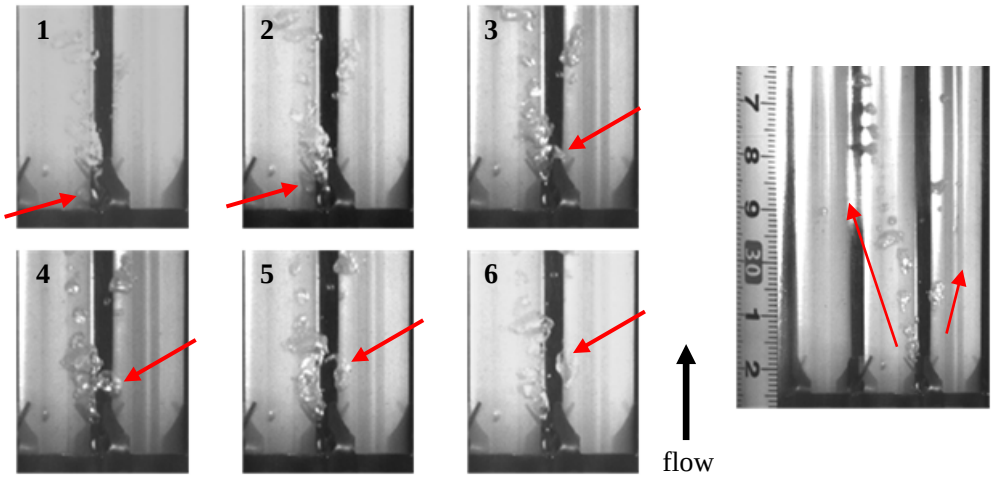

Figure 9 Photograph of the movement of bubbles from the windward of mixing vane.

Although the interface of stagnation bubble was waving with liquid flow, the size of stagnation bubble always kept constant under steady two phase flow conditions, and stagnation bubble size and the size of break-up bubbles were dependent on both liquid flow rate and void fraction, which is shown in Figure 10. As the liquid flow rate was increased with constant void fraction, the stagnation bubble size increased with smaller break-up bubbles. While the the stagnation bubble size kept fixed under different void fraction with constant liquid flow rate, the waving of stagnation bubble interface as well as the maximum break-up bubble size increased with the increasing of the void fraction due to the increase of bubble size and number of the inflow.

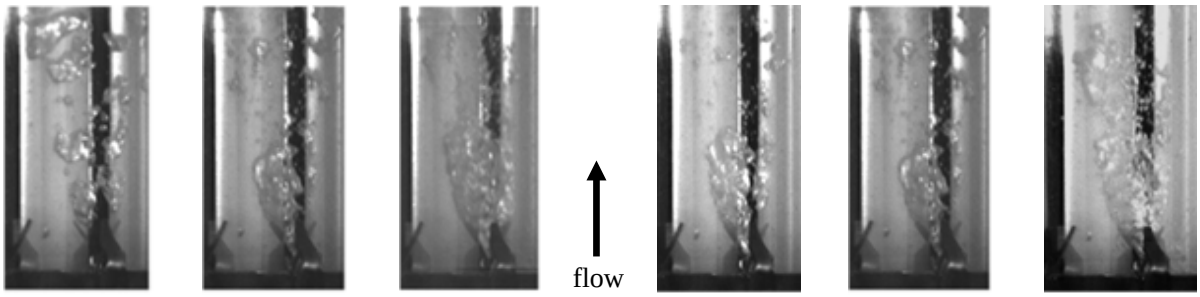

$v_{l,in}$ =1m/s $v_{l,in}$ =2m/s $v_{l,in}$ =3m/s α=0.08 α=0.12 α=0.16

a. α=0.12 b. $v_{l,in}$ = 2m/s

Figure 10 Influence of liquid flow rate and void fraction on stagnation bubble.

4.2 Numerical simulation results and discussion

The simulation of phase interface tracking was carried out in a typical subchannel with spacer grid. The standard k-ε model was selected to model the turbulence in the subchannel. More attention was focused on the bubble behaviors in the vicinity of mixing vane rather than the downstream of the spacer grid. The behaviors of bubbles at windward and leeward of mixing vane was calculated with surface tension of 0.073 N•m， contact angle of 60° and initial bubble diameter of 3.2mm.

The single bubble rising up against the windward of mixing vane expanded to the both sides, which is shown in Figure 11. At the leeward of mixing vane, the bubble rising velocity decreased without stagnation as the liquid inlet velocity was 1m/s. And as the liquid inlet velocity increased, bubble stagnation occurred with bubble break-up at the end of the stagnation bubble, which met good agreement with the visualization data. The stagnation bubble under different velocities is shown in Figure 12. At the leeward of mixing vane, the existence of a lower pressure region with lower velocity was found to maintain the bubble stagnation, as Figure 13 shows. As the liquid flow rate was increased, the region of low pressure was also enlarged to keep a larger stagnation bubble.

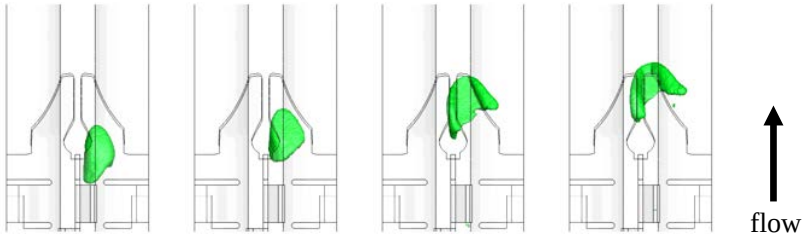

Figure 11 Numerical results of single bubble behavior at the windward of mixing vane.

The bubble behaviors in the vicinity of mixing vane in the numerical simulation met good agreement with the visualization results. In the transient numerical solution, the pressure drop of the subchannel as the bubble passing through the spacer grid was obtained, which is shown in Figure 14. The pressure drop fluctuated obviously when the bubble entered into the spacer grid and passed the mixing vane. As the bubble entering into the spacer grid, the acceleration pressure

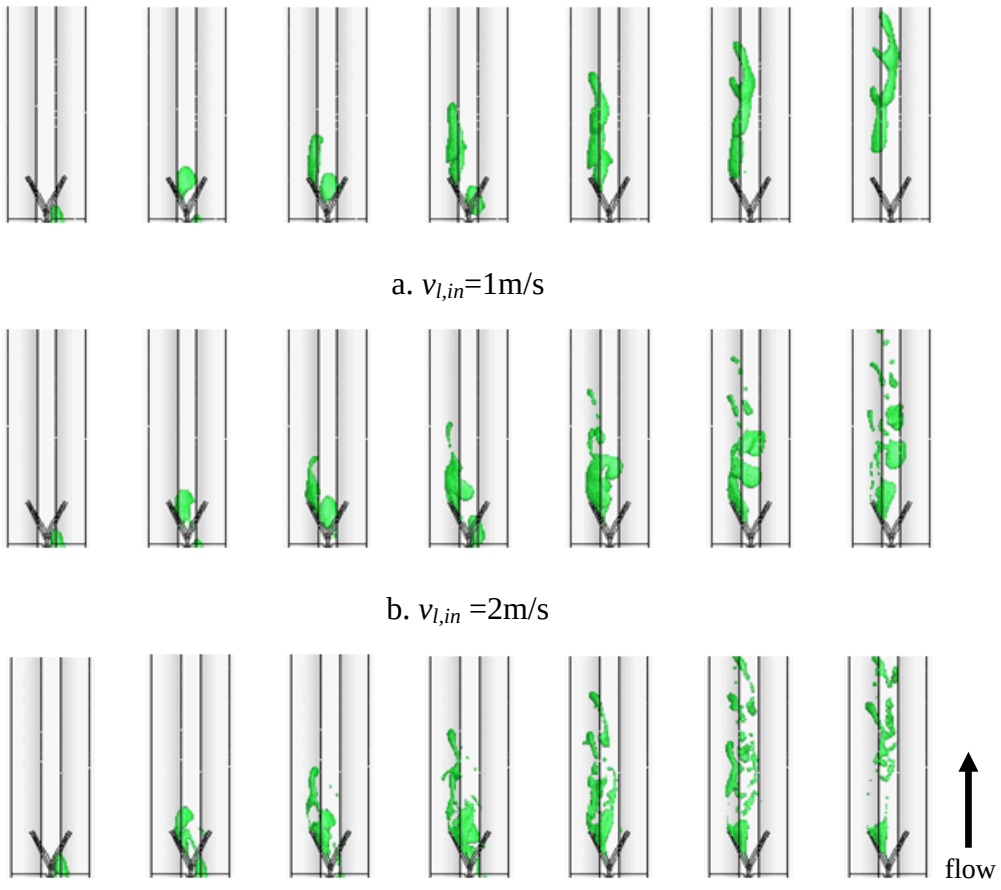

a. $v_{l,in}$=1m/s

b. $v_{l,in}$ =2m/s

c. $v_{l,in}$ =3m/s

Figure 12 Bubble stagnation under different liquid velocities with VOF method.

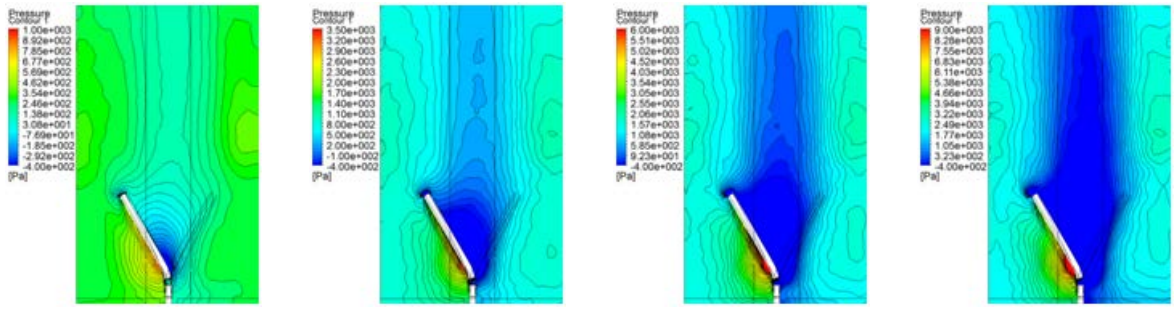

a. $v_{l,in}$ =1m/s b. $v_{l,in}$ =2m/s c. $v_{l,in}$ =3m/s d. $v_{l,in}$ =4m/s

Figure 13 Pressure contours in the vicinity of mixing vane under different flow rate.

drop generated by the different velocity distribution between the upstream and the inside of the spacer grid fluctuated due to the density difference between liquid and gas. Notably, the pressure drop of bubble before the spacer grid was the same as that in the spacer grid, which was equal to the single phase pressure drop of the subchannel. But the maximum pressure drop of bubble passing the mixing vane was higher than single phase pressure drop, resulting from that the bubble contacting with mixing vane changed local wall shear stress and local pressure drop. In this study, the inlet and outlet boundary condition was set to velocity inlet and pressure outlet, respectively. Hence, the flow rate of the subchannel kept constant as the pressure drop fluctuation occurred. If the inlet boundary condition is set to constant pressure, that is constant driven head, it seems that the fluctuation of liquid flow rate would occur, which indicates that the bubble behaviors in the vicinity of mixing vane would have influence on the local flow rate and the mass and energy transfer between the adjacent subchannels.

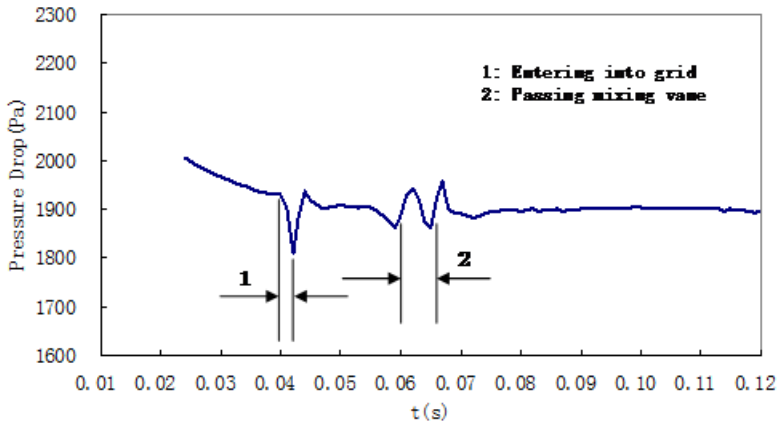

Figure 14 Influence of bubble behavior on pressure drop of the subchannel.

5. Conclusion

In this study, the visualization data of bubble behaviors in the vicinity of mixing vane was achieved by employing the FEP rods and local injecting rod in a 3×3 bundle, which eliminated interface distortion and overlapping. It was found that the bubble stagnation occurred at the

leeward of mixing vane. The stagnation bubble size increased as the liquid flow rate was increased under constant void fraction, and the interface waving of stagnation bubble increased as the void fraction was increased under constant liquid flow rate. The bubble size and phase distribution in the rod bundle were also influenced by the coalescence and break-up process with the stagnation bubble. The results of VOF method showed good agreement in the bubble stagnation with the experiment. The pressure drop fluctuation obtained from the simulation revealed the influence of bubble behaviors on the two phase flow.

6. Acknowledgements

The financial support provided by the National Natural Science Foundation of China (approved number: 51106142) is gratefully acknowledged.

7. References

[1] C.W. Hirt and B.D. Nichols, “Volume of Fluid (VOF) method for the dynamics of free boundaries”, J.Comput.Phys., 39, 1981, pp. 201-225.

[2] L. Chen, S.V. Garimella, J.A. Reizes, E.Leonardi, “The development of a bubble rising in a viscous liquid”, J.Fluid Mech., vol.387, 1990, pp. 61-96.

[3] H. Wang, Z.Y. Zhang, Y.M. Yang, H.S. Zhang, “Viscosity effects on the behaviour of a rising bubble”, Journal of Hydrodynamics, 22(1), 2010, pp. 81-89.

[4] R.H. Chen, W.X. Tian, G.H. Su, S.Z. Qiu, Yuki Ishiwatari, Yoshiaki Oka, “Numerical investigation on coalescence of bubble pairs rising in a stagnant liquid”, Chemical Engineering Science, 66, 2011, pp. 5055-5063.

[5] Y.Q. Zu, Y.Y. Yan, S. Gedupudi, T.G. Karayiannis, D.B.R. Kenning, “Confined bubble growth during flow boiling in a mini-/macro-channel of rectangular cross-section Part II: Approximate 3-D numerical simulation”, International Journal of Thermal Sciences, 50, 2011, pp. 267-273.

[6] S.S. Jeon, S.J. Kim, G.C. Park, “Numerical study of condensing bubble in subcooled boiling flow using volume of fluid model”, Chemical Engineering Science, 66, 2011, pp. 5899-5909.

[7] S.Senthilkumar, Y.M.C. Delaure, D.B. Murray, B. Donnelly, “The effect of the VOF-CSF static contact angle boundary condition on the dynamic of sliding and bouncing ellipsoidal bubbles”, International Journal of Thermal Sciences, 32, 2011, pp. 964-972.

[8] D.L. Youngs, “Time-dependent multi-material flow with large fluid distortion”, Numerical Methods for Fluid Dynamics, K.W. Morton and M.J. Baines, editors Academic Press, 1982.

[9] J.U. Brackbill, D.B. Kothe, C. Zemach, “A continuum method for modelling surface tension”, J.Cpmput.Phys., 100, 1992, pp. 335-354.